Journal of Molecular Graphics and Modelling 61 (2015) 44–52

Contents lists available at ScienceDirect

Journal of Molecular Graphics and Modelling

journal homepage: www.elsevier.com/locate/JMGM

A comparative study of binding affinities for 6,7-dimethoxy-4-pyrrolidylquinazolines as phosphodiesterase 10A inhibitors using the linear interaction energy method

Erik Rosendahl Kjellgren [1], Oliver Emil Skytte Glue [1], Peter Reinholdt [1], Julie Egeskov Meyer, Jacob Kongsted, Vasanthanathan Poongavanam *

Department of Physics, Chemistry and Pharmacy, University of Southern Denmark, Odense M, Denmark

ARTICLE INFO

Article history:
Received 7 April 2015
Received in revised form 5 June 2015
Accepted 20 June 2015
Available online 29 June 2015

Keywords:
Phosphodiesterase 10A
Schizophrenia
Pyrrolidylquinazoline
Binding affinity
Linear interaction energy
Virtual screening and applicability domain

ABSTRACT

The linear interaction energy (LIE) method was used to estimate the free energies of binding for a set of 27 pyrrolidylquinazoline derivatives as phosphodiesterase 10A inhibitors. Twenty-six X-ray crystal structures of phosphodiesterase 10A and two sampling methods, minimization and Hybrid Monte Carlo, were used to assess the affinity models based on the linear interaction energies. The best model was obtained based on the parameters $\alpha = 0.16$ and $\beta = 0.04$, which represent non-polar and polar interactions, respectively, with a root mean square error (RMSE) of 0.42 kcal/mol ($R^2 = 0.71$) and 0.52 kcal/mol ($R^2 = 0.86$) for the training and test sets, respectively. In addition, the applicability domain of the model was investigated. After validation of the models, the best model was subsequently used in a virtual screening process, which resulted in a set of optimized compounds. The models developed in this study could be useful as filter for virtual screening and lead optimization processes for phosphodiesterase 10A drug developments.

1. Introduction

Phosphodiesterases (PDEs) form an ubiquitous family of enzymes that play a crucial role in the breakdown of phosphodiester bonds in cyclic nucleotides. On the basis of their structural topologies and locations each of these PDEs show different clinical importance [1,2]. From a pharmaceutical point of view, potential inhibitors of any of these PDEs have high therapeutic importance, for example in relation to schizophrenia (PDE10) [3].

PDE10 is a protein located widely across many parts of the body. However, PDE10A is most dense in the medium spiny neurons, striatum and basal ganglia [4,5]. PDE10A inhibitors prevent hydrolysis of cyclic adenosine monophosphate (cAMP) and cyclic guanosine monophosphate (cGMP) to adenosine monophosphate (AMP) and guanosine monophosphate (GMP), respectively. In the basal ganglia dopamine D2 can also be found at high density. Due to this, the striatum is thought to be a central complex in the "dopamine hypothesis of schizophrenia". According to this hypothesis, many of the antipsychotics drugs that are used for schizophrenia in human have dopamine antagonistic effects (especially the D2 receptor). In this context, PDEs inhibitors are shown to regulate the dopamine cAMP/PKA (cyclic adenosine monophosphate dependent protein kinase A) signaling pathways either directly (i.e. activate the D1 receptor signaling) or indirectly (i.e. inhibits the D2 receptor signaling) [6–8]. In humans two major PDE10 variants have been reported, i.e. PDE10A1 and PDE10A2 [9–11]. The PDE10A1 protein consists of 779 amino acids and residues Thr364, Gln383, His515 and Gln716 form the ligand-binding site (allosteric/active site). His519, His553, Asp554 and Asp664 coordinate with a Zinc ion and mutation of any of these residues abolish or reduce the enzyme catalytic activity [12,13]. This effect is due to the fact that these residues provide a favorable environment for metal ion stabilization. The active site is well characterized from X-ray crystallography as being small (<300 Å^2) and relatively polar [12,13]. A large number of PDE10 inhibitors have been reported (including Papaverine) [14–21], and currently more than 180 patent applications have been published [22]. Many of these are in various stages of clinical trials, but none of these inhibitors have yet reached the market [7,23]. Searching for selective and potent inhibition of PDE10 is greatly needed to treat schizophrenia, therefore, any procedures that speed up the screening process could potentially be used in the drug discovery process.

* Corresponding author. Fax: +45 66158760.
E-mail address: nathan@sdu.dk (V. Poongavanam).
[1] These authors contributed equally to this work.

http://dx.doi.org/10.1016/j.jmgm.2015.06.010
1093-3263/

In the present study, we have developed binding affinity models for PDE10 inhibitors using the linear interaction energy (also linear response or LIE) method [24,25]. Special attention has been paid to evaluate different sampling methods including minimization and hybrid Monte Carlo (HMC). Moreover, LIE models based on a large number of X-ray crystal structures of PDE10 were developed in order to validate and compare the quality of the binding affinity models based on different X-ray crystal structures. Some of these structures have no bound ligands which result in different conformations compared to the structures with bound ligands particularly in the PDE10 active site. It has previously been shown that different X-ray crystal structures yield different model quality [26]. Moreover, in this investigation, we did not perform extensive molecular dynamic (MD) simulations; rather, different conformations of the protein-ligand structures were explored in order to suggest which PDE10 structures give better results using simpler computational methods such as energy minimization based on a single structure and HMC.

2. Computational methods

2.1. Binding affinity calculations

Accurate prediction of binding affinities for ligands is a major challenge in computer-aided drug design and in particular in lead identification/optimization processes [27]. For this, a large number of computational methods have been developed [28,29]. Very often docking and scoring functions have been used to assess the binding affinity of large datasets because these methods are computationally inexpensive. However, these methods poorly rank the ligands according to their experimental activity. Therefore, it is highly relevant to develop an affinity prediction model that is capable of being both relatively accurate and applicable to a large number of compounds. The linear interaction energy (LIE) method is a linear response theory based method [30–32].

The LIE method requires calculation of average interaction energies between the ligand and its surroundings based on either molecular dynamics (MD), Monte Carlo simulations or energy minimization based on a single structure of the ligand in solution and when bound to the protein [24,25]. The binding free energy is subsequently estimated using the following expression:

$$\Delta G_{\text{Bind}} = \alpha\langle\Delta U_{\text{vdW}}\rangle + \beta\langle\Delta U_{\text{el}}\rangle + \gamma\langle\Delta U_{\text{Cav}}\rangle$$

In this equation, the angle brackets (< >) denote ensemble average of the intermolecular electrostatic (el) and van der Waals (vdW) energies of the ligand with its surroundings in the bound and free states. The parameters of this equation are the coefficients α and β for the nonpolar and polar contributions to the binding free energy, respectively, and γ is an additional constant. In the original derivation, γ was not included, the value of α was derived from linear response to be 0.5, and β was empirically determined to be 0.16 [30]. More recent studies by Zhou et al. [33] and others [34,35] have reformulated the original expression by adding a third parameter called the cavity term (which is a parallel to the cavity energy in continuum solvent models) to the fit.

In the present study, we have used the Liaison [36] tool from the Schrödinger suite [37] for the LIE calculations. The Liaison tool provides three sampling procedures in order to get interaction energies for the ligand binding. These procedures are (i) energy minimization, (ii) hybrid Monte-Carlo (HMC) and (iii) molecular dynamic simulation (MD). Each of these methods offers different level of sampling. For instance, the MD based sampling is often used to calculate the interaction energies for LIE models because MD based methods considers the full protein and ligand flexibility, which allows to capture large conformational changes in the course of ligand binding. However, such a sampling protocol is generally very time consuming, expensive and inefficient to handle a large number of compounds. Energy minimization based on a single structure and hybrid Monte Carlo (HMC) based protocols not only offers greater reduction in computational efforts, but in some case, also performs equally good as the MD based sampling methods.

The conformational sampling based on HMC is relatively efficient compared to the MD simulation [38]. HMC sampling makes a short series of molecular dynamics steps, and then uses a standard Metropolis "Monte Carlo" test to decide whether to accept the new geometry or to go back and try again [36]. Liaison uses the Surface Generalized Born (SGB) continuum solvation model with the OPLS 2005 force field. In the minimization steps, a 12 Å region of the protein around the ligand was treated flexible, while the region between 12 to 16 Å was restrained [39].

Table 1
Compounds used for the binding affinity calculation

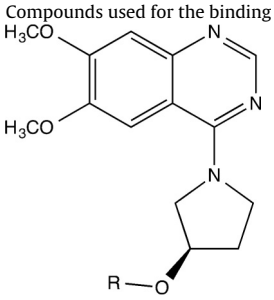

Cpd. No.	R Substitution	K_i (μM)	$\Delta G_{\text{Exp.Bind}}$ (kcal/mol)
1	2-Quinoxalinyl	0.004	−11.53
2	2-Naphthyl	0.012	−10.87
3	6-Quinolinyl	0.012	−10.87
4	7-Quinolinyl	0.012	−10.87
5	2-(7-Methoxynaphthyl)	0.017	−10.66
6#	2-(6-Methoxynaphthyl)	0.018	−10.63
7#	6-(2-Methylquinolinyl)	0.018	−10.63
8	3-Isoquinolinyl	0.019	−10.60
9	5-Chloro-2-pyrimidinyl	0.044	−10.10
10	4-Ethoxyphenyl	0.054	−9.98
11	4-Cyanophenyl	0.056	−9.95
12	3-4-Dimethoxyphenyl	0.067	−9.85
13#	5-(2-3-Dihydro-1H-indenyl)	0.068	−9.84
14	3-Ethoxyphenyl	0.094	−9.64
15	4-tert-Butylphenyl	0.100	−9.61
16	4-Pyridinyl	0.112	−9.54
17#	2-Pyridinyl	0.123	−9.48
18	3-Pyridinyl	0.128	−9.46
19	2-Cyanophenyl	0.130	−9.45
20	3-Biphenyl	0.136	−9.42
21#	3-i-Propylphenyl	0.171	−9.29
22	4-Trifluoromethoxyphenyl	0.185	−9.24
23#	2-Chlorophenyl	0.198	−9.20
24	1-Naphthyl	0.210	−9.17
25	2-Methoxyphenyl	0.240	−9.09
26	2-Methylphenyl	0.326	−8.90
27	2-Trifluoromethylphenyl	0.811	−8.36

Note: $\Delta G_{\text{Exp.Bind}}$ is calculated using $\Delta G_{\text{bind}} = -RT \ln (K_i)$ (R is the gas constant and T is the absolute temperature). Compounds indicated with # are used as validation (test set) dataset.

3. Preparation of ligand–protein complexes

A set of 6,7-dimethoxy-4-pyrrolidylquinazoline derivatives with known K_i values (Table 1) was collected [40]. Here K_i denotes the measure of inhibitors binding affinity to the enzyme. The structures were prepared with the LigPrep [41] tool from the Schrödinger Suite [37]. Epik [42] was used to determine the ionization state of the molecules (at pH 7.0).

There were at least 69 X-ray crystal structures of PDE10A from the Protein Data Bank at the time of this study. Thus structures

with a resolution of less than 2 Å were selected for the study (26 structures) in order to evaluate the binding affinity models from the different structures and furthermore to propose the structures that are suitable for virtual screening (supporting material, TS1). The protein structures were prepared with the Protein Preparation Wizard [43] from the Schrödinger Suite (using default settings, i.e., assign bond order and adding missing hydrogen atoms to the protein structures). The ionization states of the structures were predicted with the PROPKA [44] tool for a pH of 7.0. Finally, the structures were subjected to a heavy atom restrained minimization (i.e., only the hydrogen atoms are optimized), Heavy atom restrained minimization was performed using the Impact tool as implemented in the Schrödinger Suite [39].

The protein-ligand complexes of the compounds under investigation were obtained from Glide [45] docking with the XP (Extra Precision) scoring function (default settings for finding the starting poses). The diameter midpoint of each docked ligand were allowed to vary 16 Å in each direction, the maximum length were increased to 36 Å to allow any ligands to be docked.

The binding free energy (ΔG_{bind}) from K_i was estimated using $\Delta G_{bind} = -RT \ln(K_i)$. Here, R is the gas constant and T is the absolute temperature. The obtained binding free energy for the series ranges from −11.53 to −8.36 kcal mol^{-1}. Of a total of 27 compounds, 6 compounds were used as an internal test set and the remaining 21 compounds were used to train the binding affinity models. In our study we used the same training and test set compounds as in a previous study based on 3D-QSAR [40] (Fig. 1). This is done in order to be able to compare directly the outcome of the two model approaches.

The quality of the LIE model was assessed in terms of root-mean-square-error (RMSE) and the correlation coefficient (R^2) of the test set. In addition, the Jackknife method based on leave-one-out (LOO) cross validation was also performed.

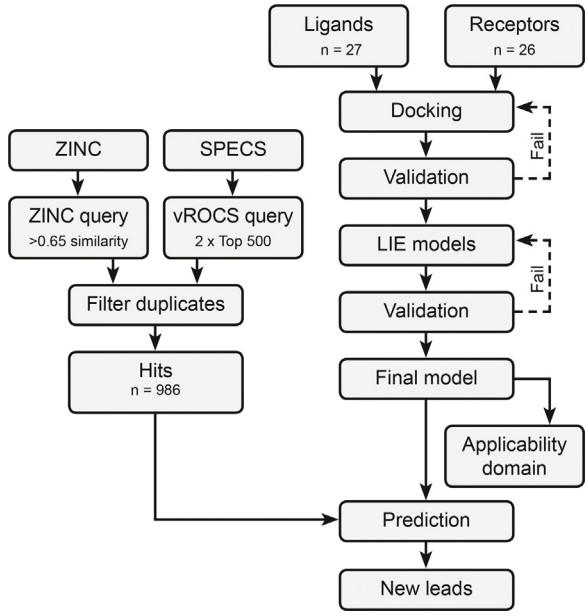

Fig. 1. The overall workflow in the present study.

4. Results and discussion

4.1. Validation of docking protocol

The validity of the docking settings were first assessed by the ability of the docking method to reproduce the X-ray crystal bound ligand conformation for each crystal structure. In most cases, the root-mean square deviation (RMSD) between the crystal bound and the docking pose yields an RMSD of less than 1 Å (Fig. 2). Some crystal structures, for instance, 4MRW, 4LLX, 4LLJ showed very high RMSD in the first ranked pose, and these high RMSDs did not improve up to the top 10 binding poses from the XP docking protocol (see Supplementary, TS2).

It has previously been shown that inhibitors show strong interactions with hydrophobic residues and especially with Phe686, Leu622, Leu625 and Phe719. Additional hydrogen bonding between the N-atom of quinoxaline with Gln716 is also found. As shown in the X-ray crystal structures, the docking poses also show these crucial interactions particularly His519, Asp552, His553, Glu582 and Asp664 all coordinate with the metal ion (Fig. 2B). Additionally, protein structure alignment was performed with all X-ray crystal structures in order to check the conformational differences of the backbone as well as the position of metal ion and active site residues. This revealed that the active site and metal ion position are relatively stable (RMSD less than 1 Å).

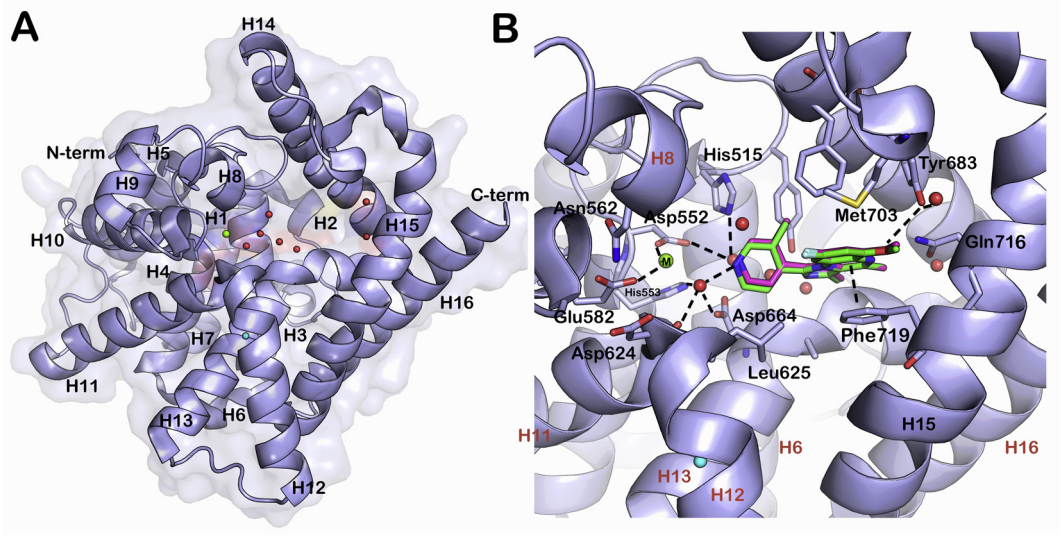

Fig. 2. Cartoon representation of the PDE10A structure with X-ray crystal bound ligands (sticks) and metal (green sphere). The active site is highlighted in the right panel. The binding mode of PDE10A inhibitor from docking solution (green stick) is compared to crystal bound conformation (pink stick). PDB ID: 3SN7.

Table 2
Summary of the two-and-three parameter LIE models for structures using the minimization procedure.

PDE10A structures	Parameters (2)		Training		Test		Parameters (3)			Training		Test	
	α	β	RMSE	R^2	RMSE	R^2	α	β	γ	RMSE	R^2	RMSE	R^2
2OUN	0.258	0.093	0.968	0.094	0.438	0.682	0.174	0.081	−0.656	0.835	0.256	0.365	0.745
2OUP	0.262	0.043	0.940	0.093	0.556	0.360	0.194	0.044	−0.484	0.836	0.226	0.235	0.852
3SNI	0.214	-0.049	0.719	0.203	0.927	0.082	0.176	−0.041	−0.371	0.681	0.274	0.721	0.241
4HEU	0.158	0.042	0.422	0.713	0.518	0.858	0.149	0.041	−0.125	0.414	0.733	0.527	0.865
4LLK	0.208	0.049	1.550	0.282	1.923	0.528	0.092	−0.023	−1.167	0.472	0.665	0.444	0.452
4LM0	0.215	−0.093	0.600	0.417	0.394	0.799	0.167	−0.110	−0.493	0.555	0.505	0.387	0.696
Average	0.209	0.010	0.954	0.143	0.830	0.325	0.134	0.002	−0.754	0.728	0.317	0.588	0.516
Std. Div.	0.024	0.069	0.264	0.175	0.355	0.292	0.036	0.051	0.348	0.141	0.171	0.210	0.310

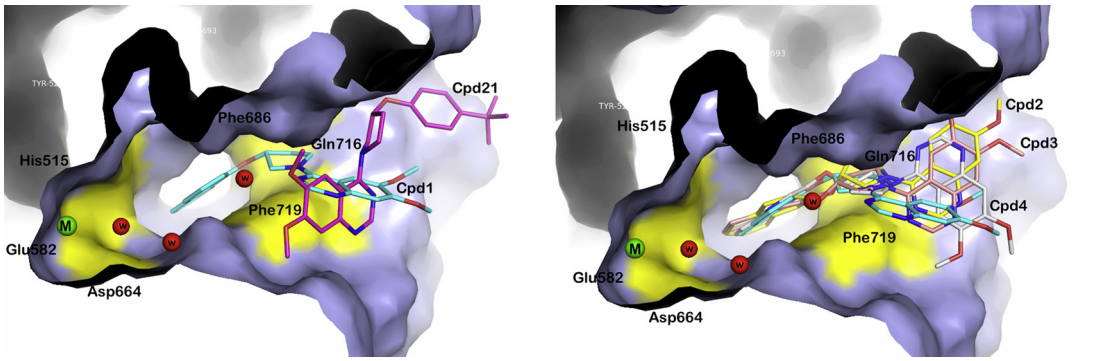

Fig. 3. The binding mode of compound 1(cyan), 21 (pink), 2 (yellow), 3 (maroon) and 4 (white) is compared and important residues arealso highlighted including metal and water molecules (PDB ID: 4LLK). (For interpretation of the references to color in this figure legend, the reader is referred to the web version of this article.)

4.2. Binding affinity models

The binding interaction energies for each X-ray crystal structure using the energy-minimization and hybrid Monte-Carlo (HMC) sampling procedures were calculated as implemented in the Liaison tool in the Schrödinger suite [36]. Subsequently the LIE models were developed and assessed (so called two- and three-parameter models). In this work, for every structure, the standard LIE models were also developed, (i.e., by using the default LIE parameters), however, due to insignificant quality only the optimized models were reported and discussed.

As stated before, a set of 21 compounds was used as training set and the remaining 6 compounds were used as a test set. The quality of the LIE models was assessed using the root mean square error (RMSE) and correlation coefficient (R^2) of the test set. A summary of the LIE models (two-parameter) is provided in the Table 2 (Summary of developed models for each structures is provided in the supporting information, ST3). In general, the quality of the optimized LIE models for all crystal structures was relatively good and showed RMSE of less than 2 kcal/mol for the test set. The model from the crystal structure 4LM0 is found to be better than the other structures and showed an RMSE of 0.60 kcal/mol (R^2 = 0.41) for the training set and 0.39 kcal/mol (R^2 = 0.80) for the test set. Very similar performance was observed for the 4HEU structure with an RMSE of 0.42 kcal/mol (R^2 = 0.71) for the training and 0.52 kcal/mol (R^2 = 0.85) for the test set. A clear outlier is cpd 21 which is one of the low active compounds in the series, but this compound was predicted falsely as a highly active compound with a binding affinity of −12.2 kcal^{-1}mol (for 4LLK). A binding mode analysis of cpd 21 reveals that the receptors interaction with this compound is quite different as compared to compounds that are predicted correctly in most of the models (Fig. 3).

In general, the LIE models from the HMC method perform very similar to the results obtained from the minimization procedure in both the two- and three-parameter models (Table 3, Fig. 4) (Summary of developed models for each structures is provided in the supporting information, ST4). In the two-parameter scenario, especially, predictions from based on the structures 3OUP, 3SNI and 4HEU are remarkably good with an RMSE of <0.50 kcal/mol (R^2 > 0.7) for the test set. Some of the models from the remaining structures also lie within the statistically acceptable threshold (RMSE < 1 kcal/mol).

Moving to the three-parameter model we obtain an average α = 0.13 and an insignificant value of β, however, we obtain a

Table 3
Summary of the two-and-three parameter LIE models for structures using the HMC procedure.

PDE10A Structures	Parameters (2)		Training		Test		Parameters (3)			Training		Test	
	α	β	RMSE	R^2	RMSE	R^2	α	β	γ	RMSE	R^2	RMSE	R^2
2OUN	0.27	0.07	1.12	0.03	0.60	0.74	0.14	0.05	−0.98	0.81	0.32	0.41	0.77
2OUP	0.23	0.01	0.66	0.34	0.67	0.17	0.15	0.01	−0.71	0.56	0.50	0.63	0.29
2OUQ	0.28	0.06	1.05	0.08	0.35	0.78	0.17	0.05	−0.73	0.80	0.31	0.47	0.85
3SNI	0.21	0.01	0.63	0.41	0.35	0.91	0.16	0.00	−0.56	0.55	0.51	0.38	0.82
4HEU	0.17	0.03	0.49	0.68	0.45	0.86	0.15	0.03	−0.27	0.46	0.73	0.45	0.88
4LKQ	0.22	0.10	0.93	0.25	0.64	0.70	0.15	0.07	−0.65	0.82	0.41	0.54	0.86
4LLK	0.21	−0.01	1.51	0.27	1.90	0.56	0.10	-0.05	−1.13	0.50	0.63	0.53	0.26
Average	0.22	0.01	0.98	0.17	0.85	0.37	0.13	0.00	−0.84	0.73	0.36	0.61	0.50
Std. Div.	0.03	0.06	0.25	0.17	0.36	0.32	0.03	0.04	0.32	0.14	0.16	0.19	0.29

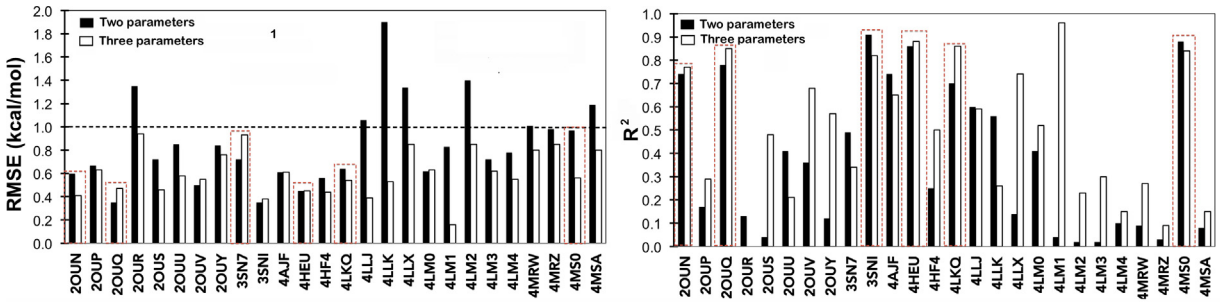

Fig. 4. Comparison of test set prediction from two-and-three-parameter fit using the HMC procedure.

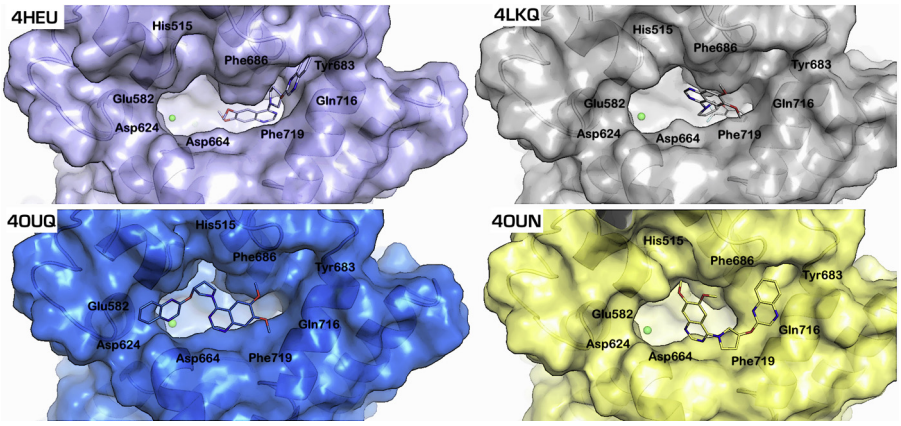

Fig. 5. Comparison of binding modes of cpd 1 in PDE10A in different X-ray crystal structures.

large and negative contribution of γ (average $\gamma = -0.84$). Here, the cavity energy term refers to the energy obtained from an exposed surface area of the ligand by contact with the receptor (i.e. $\langle U^{bound}{}_{cav}\rangle - \langle U^{free}{}_{cav}\rangle$). The negative contribution of the cavity term indicates that the unfavorable energy from the ligand cavity seems to play an important role in the binding affinity of this class of PDE10A inhibitors. Furthermore, the small contribution of the electrostatic term in the LIE models is due to lack of hydrogen bonding or salt bridge interactions between the ligand and receptors, conversely π–π interactions (mainly with Phe719) dominates the overall binding energy and no noticeable electrostatic interactions were found. In comparison to the models from the two-parameter fit, three-parameter models showed significantly better performance, both in terms of the RMSE and correlation coefficient between the observed and predicted binding affinities.

It is clear from Fig. 5 that the quality of the model is slightly affected when the structure is co-crystallized with inhibitors compared to the use of structures without co-ligand i.e., apo structures (2OUN and 2OUQ) and ligand bound structures (4HEU and 4LKQ). As seen from Fig. 5, one of the highly active compounds (cpd 1) exists in four different binding modes, however, the binding modes from the 4HEU and 4LKQ structures are quite similar in the way that the quinoxalinyl ring is inserted deep into the binding pocket which favors the strong π–π interaction with Phe719. In the apo structures, the ligand cannot enter deeply into the binding pocket and eventually lacks the essential hydrophobic interaction. Although there is no significant flexibility on the surface of the receptor, the conformation of Gln716 deep in the pocket seem to play a significantly role in ligand recognition (Fig. 6) [12]. Particularly in the apo structures Gln716 is tightly locked with hydrogen bonding to the substrate (AMP), which gives rise to a different conformation of the binding pocket as compared to the structures with the co-ligand bound.

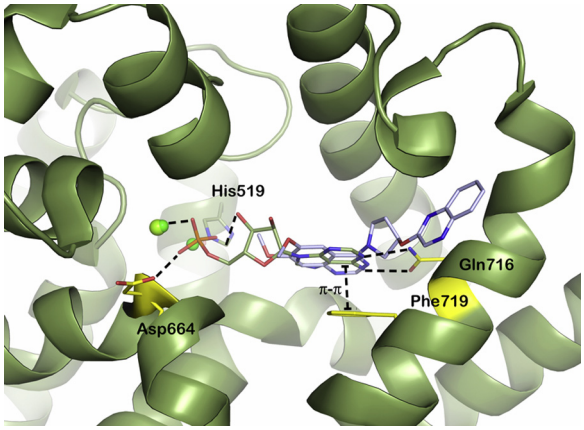

Fig. 6. The comparison of binding mode of cpd 1 with crystal bound PDE10A substrate (AMP) (PDB ID: 2OUN), important residues are highlighted including metal and interactions.

Although the models obtained from either minimization or hybrid Monte Carlo (HMC) yields similar quality, from a computational efficient point of view, the models based on the minimization procedure are clearly more suitable for virtual screening of PDE10A inhibitors from a large chemical database. Furthermore, out of the 26 receptor structures used for the binding affinity calculation, the models from the 4HEU structure are very consistent in both sampling procedures as well as in the LIE parameter optimization scenarios (two- and three-parameter). Thus for our virtual screening procedure we used the 4HEU structure. The correlation between experimental and calculated binding affinities from the 4HEU structure with the three-parameter LIE model is shown Fig. 7.

Table 4
Comparison of binding affinity models.

Methods	Models	Contribution	Components /parameters	Training		Test
				R^2	R^2_{cv}	R^2
CoMFA	1	Steric	2	0.82	0.415	0.31
CoMFA	2	Steric	5	0.99	0.557	0.92
LIE	4HEU	vdW	2	0.71	0.715¶	0.86
LIE	4LM1	vdW	3	0.45	0.441¶	0.84

Note: ¶ Leave-one-out (LOO) cross validation using the Jackknife technique.

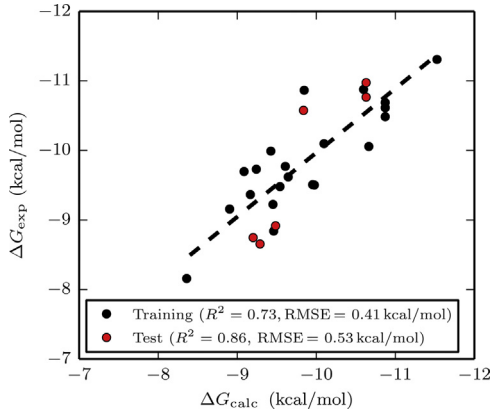

Fig. 7. Correlation between the calculated and observed binding free energies using the empirical model (4HEU).

4.3. Comparison with previous binding affinity models

The dataset used in this study has previously been used for ligand based 3D-QSAR methods such as CoMFA and H-QSAR [40]. It is therefore of interest to compare both the CoMFA model and LIE binding affinity models. The best CoMFA model showed a correlation coefficient of 0.991 (std = 0.24) for the training and 0.919 (std = 0.065, principle components (PC) = 5) for the test set. Our best models were obtained from the three-parameter LIE models that showed remarkably low RMSD 0.4 to 0.85 kcal/mol (R^2 = 0.022–0.73) for the training and 0.23 to 0.56 kcal/mol (R^2 = 0.45–0.89) for the test set. From a direct comparison in terms of statistical significance, the CoMFA model is slightly better than the LIE models, however, the previous CoMFA model uses five principle components for 21 compounds which might leads to chance correlation problem according to the "rule-of-thumb" or "rule-of-five" [46] (at least five data points per structural descriptors or component) in order to be statistically significant for future prediction. Based on this observation, our binding affinity model is not only simpler than the CoMFA model but also provides structural interaction information. Moreover, both models suggest that the overall binding affinity of this class of compounds to PDE10A is mainly governed by the non-polar interactions and not electrostatic interactions (Table 4).

4.4. Applicability domain

In addition to the binding affinity models, an applicability domain (AD) experiment was performed to check the reliability of the developed affinity models for future prediction [47]. AD provides a first structural alert on the dataset and is primarily used to check whether a new molecular entity is within the chemical space of the training set or not. For the AD experiment a set of 160 PDE10 inhibitors was retrieved from ChEMBL database [48] and this dataset consist of 6 different scaffolds [19,49–53] which share no structural similarity with the training set that we used for the binding affinity model development [40]. The ΔG_{obs} values span an energy difference of 3.16 kcal/mol (Fig. 8A). In each case, the energies were calculated with Liaison and statistical parameters were calculated with the model (M) and optimal (N) α and β parameters (Fig. 8B). The optimal parameters were fitted to produce the lowest RMSE, so the value of R^2 is seen to decrease in some cases. In four cases, the model RMSE values are below the ΔG_{obs} energy span, and the RMSE difference is below 25% in three cases. The model is not suited for all clusters, which can be seen from the high value of RMSE at PubMed ID 22227212. The R^2 value is low in all cases. This could be caused by the narrow interval of ΔG_{obs}. Thus the model is able to differentiate active from inactive compounds, but it is unable to rank the active compounds in a narrow ΔG interval.

4.5. Identification of new compounds from binding affinity based virtual screening

In order to assess the LIE based binding affinity model as a useful approach for virtual screening (VS), we further tested the best

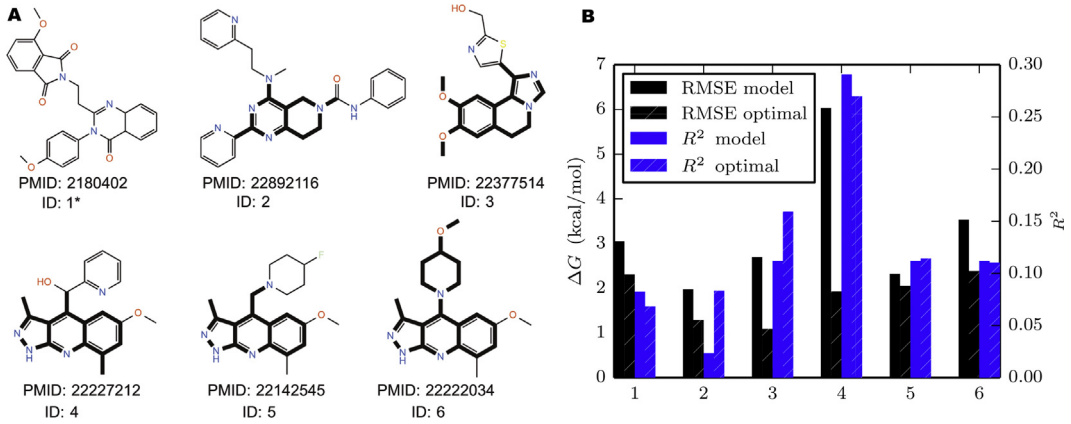

Fig. 8. (A) Representative scaffolds used for applicability domain experiment and (B) Summary of the applicability domain analysis, RMSE values (left-axis), R^2 (right-axis).

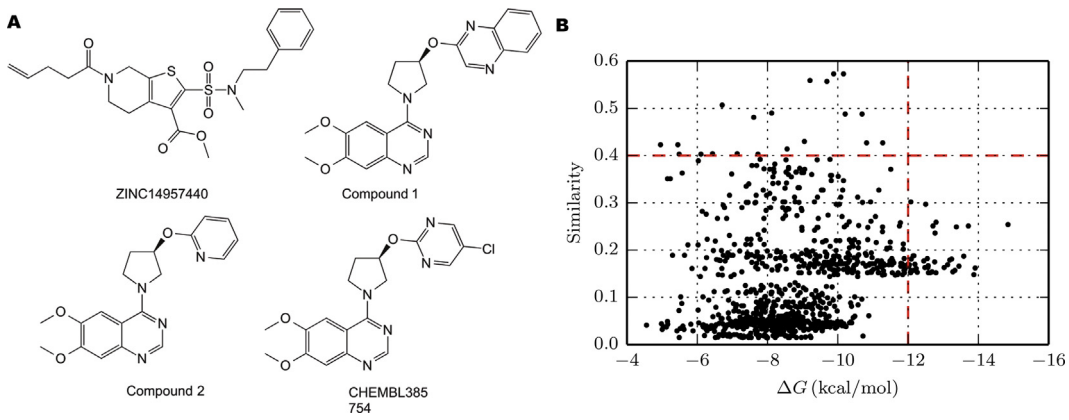

Fig. 9. A comparison of similarity score with calculated binding affinity (ΔG_{calc}) of hits (A), areas of interest is highlighted with line (B).

Table 5
Summary of top ranked compounds for PDE10A inhibition optimization.

Sr. No	Compound ID	Similarity	ΔG $_{Pred.Bind}$ (kcal/mol)	Docking score
1	ZINC27204775	0.254	−14.89	−9.05
2	ZINC82118559	0.162	−13.97	−8.60
3	ZINC82125037	0.148	−13.92	−7.16
4	ZINC27202118	0.251	−13.77	−7.32
5	ZINC82119374	0.187	−13.62	−5.61
6	ZINC82129362	0.166	−13.50	−9.28
7	ZINC27209199	0.249	−13.41	−8.78
8	ZINC82125604	0.157	−13.39	−9.73
9	ZINC82125041	0.154	−13.34	−10.24
10	ZINC82136446	0.181	−13.28	−7.59
11	ZINC82125221	0.179	−13.18	−8.71
12	ZINC82124938	0.169	−13.12	−7.95
13	ZINC82129453	0.163	−13.02	−10.39
14	ZINC27203743	0.259	−12.79	−4.33
15	ZINC82125049	0.152	−12.79	−9.01
16	ZINC27215947	0.236	−12.76	−5.44
17	ZINC82131518	0.175	−12.75	−8.13
18	ZINC27202125	0.251	−12.70	−6.96
19	ZINC82125038	0.154	−12.68	−9.35
Query 1	ZINC14956507	–	−10.16	−7.69
Query 2	ZINC38279846	–	−10.78	−6.95
Standard	Papaverine	–	−7.88	−5.97

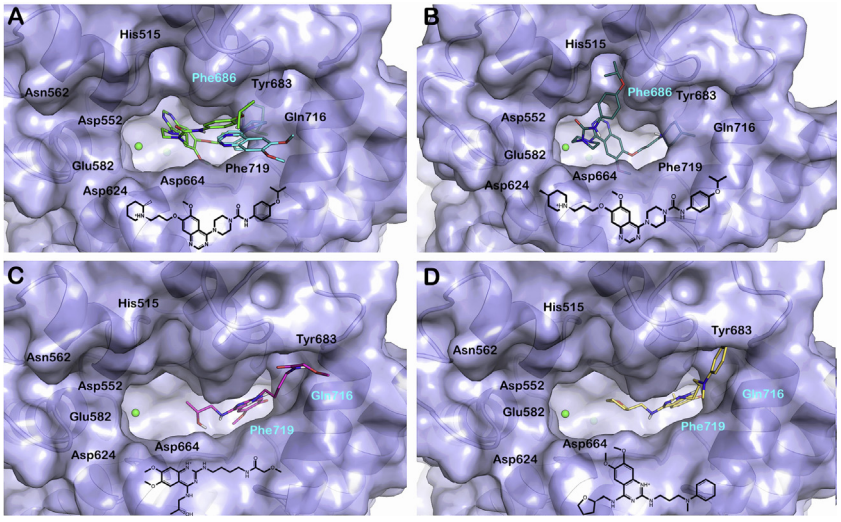

Fig. 10. Comparison of binding mode of query molecule and newly identified hits (cpd id A: ZINC27204775, B: ZINC27202125, C: ZINC82118558, D: ZINC82125037). Important residues are highlighted including metal ion. Residues that are marked in cyan symbolize the specific interaction with the ligand.

LIE model (two-parameter model, 4HEU) with the ZINC database as a compound source [54]. All the compounds were preprocessed as described in the method section. In this study, four active compounds were used as a template for the virtual screening process. In this, compound 1 (query 1) and ZINC14957440 were used as a query molecule in the ZINC [55] based similarity web search and compound 17 (query 2) and CHEMBL385754 were used as a query molecules in the vROC based shaped similarity search with SPECS database [55,56]. From the shape and ZINC based VS results, top 500 compounds for each template were saved for the binding affinity calculation. A similarity threshold of 0.65 was applied for all query molecules during the ZINC search and top 1000 compounds were chosen from the vROC based shape screening (see Fig. 1 and Fig. 9A).

Prior to use these compounds for binding affinity assessment, the hits from both screening were merged and duplicates were removed ($n = 688$) from the pool. In addition, a fingerprint based similarity metric is also calculated using Canvas [57] (Daylight invariant atom types was used). Subsequently, the top ranked compounds were analyzed on the basis of diversity and binding affinity for further binding mode analysis (Table 5, Fig. 9). The binding affinity for binders lies between −14.89 kcal/mol and −4.0 kcal/mol. Looking at the number of compounds which lie on the favorable energy scale, a large number of the compounds have been predicted as moderate binders (energy ranges from −6.0 kcal/mol to −12.0 kcal/mol) and only a limited number of similar compounds (in respect to query) are lying within this region. However, the interesting region in this plot is the region with less similarity score and stronger binding affinity (60 compounds are lying in this region).

Finally, the binding modes of the identified compounds were analyzed. From this it seems that most of the identified compounds are inserted deeply into the binding pocket, which favors the π–π interaction with Phe686, Phe719 (Fig. 10). Furthermore, it was observed that most of the compounds have a relatively long tail, which occupies the free space in the binding pocket. The reason for the strong binding of these compounds towards PDE10A may arise from the van der Waals interaction as it seem to play a crucial role in the ligand binding. Additionally, we also investigated whether these hits have previously been reported for any other drug targets using the ChEMBL bioactivity database. Out of the top 20 hits, 4 compounds have previously been reported for other targets, especially strong inhibitors for the platelet-derived growth factor receptor, human stem cell growth receptor, and human tyrosine protein kinase receptor (see Supporting information, ST5).

5. Conclusion

In the present study we have developed and assessed LIE-based binding affinity models on a set of 6,7-dimethoxy-4-pyrrolidylquinazoline analogues against 26 high-resolution X-ray crystal structures. The LIE models are based on the two sampling methods simple minimization and Hybrid Monte Carlo (HMC), and were compared. Overall, models based on the minimization procedure perform equally well compared to HMC in terms of statistical significance, however, the model developments based on the minimization procedure is much faster than the HMC method. From a virtual screening point of view, highly efficient models are preferred due to the handling of a large number of compounds for prediction. Thus, we only compare the quality of the models from the minimization procedure using here two-parameter and three-parameter optimized models. In general, both three-parameter and two-parameter based binding affinity models perform equally well (4HEU: RMSE = 0.52 kcal/mol, $R^2 = 0.86$ for the two-parameter model and RMSE = 0.53 kcal/mol, $R^2 = 0.87$ for the three-parameter model), but in order to have a simpler binding affinity model, the two-parameter model is considered the best choice. Finally, a new set of PDE10A inhibitors have been identified which shows better binding affinity compared to the known compound. Therefore, these compounds could potentially be consider as new lead compounds for further PDE10A drug development.

Acknowledgements

This work has been supported by the Lundbeck Foundation, The Danish Councils for Independent Research and the Villum Foundation. The authors are also thankful to the ChemAxon and OpenEye scientific software for providing an academic license.

Appendix A. Supplementary data

Supplementary data associated with this article can be found, in the online version, at http://dx.doi.org/10.1016/j.jmgm.2015.06.010

References

[1] S.H. Francis, M.A. Blount, J.D. Corbin, Mammalian cyclic nucleotide phosphodiesterases: molecular mechanisms and physiological functions, Physiol. Rev. 91 (2011) 651–690.
[2] S. Pierre, T. Eschenhagen, G. Geisslinger, K. Scholich, Capturing adenylyl cyclases as potential drug targets, Nat Rev. Drug Discovery 8 (2009) 321–335.
[3] D.H. Maurice, H. Ke, F. Ahmad, Y. Wang, J. Chung, V.C. Manganiello, Advances in targeting cyclic nucleotide phosphodiesterases, Nat. Rev. Drug Discovery 13 (2014) 290–314.
[4] K. Fujishige, J. Kotera, H. Michibata, K. Yuasa, S. Takebayashi, K. Okumura, et al., Cloning and characterization of a novel human phosphodiesterase that hydrolyzes both cAMP and cGMP (PDE10A), J. Biol. Chem. 274 (1999) 18438–18445.
[5] V. Lakics, E.H. Karran, F.G. Boess, Quantitative comparison of phosphodiesterase mRNA distribution in human brain and peripheral tissues, Neuropharmacol 59 (2010) 367–374.
[6] A. Nishi, M. Kuroiwa, T. Shuto, Mechanisms for the modulation of dopamine d(1) receptor signaling in striatal neurons, Front. Neuroanat. 5 (2011) 43.
[7] J. Kehler, J. Nielsen, PDE10A inhibitors: novel therapeutic drugs for schizophrenia, Curr. Pharm. Des. 17 (2011) 137–150.
[8] P. Seeman, Schizophrenia and dopamine receptors, Eur. Neuropsychopharmacol. 23 (2013) 999–1009.
[9] J. Kotera, K. Fujishige, K. Yuasa, K. Omori, Characterization and phosphorylation of PDE10A2, a novel alternative splice variant of human phosphodiesterase that hydrolyzes cAMP and cGMP, Biochem. Biophys. Res. Commun. 261 (1999) 551–557.
[10] K. Fujishige, J. Kotera, K. Omori, Striatum- and testis-specific phosphodiesterase PDE10A isolation and characterization of a rat PDE10A, Eur. J. Biochem./FEBS 266 (1999) 1118–1127.
[11] K. Loughney, P.B. Snyder, L. Uher, G.J. Rosman, K. Ferguson, V.A. Florio, Isolation and characterization of PDE10A, a novel human 3′, 5′-cyclic nucleotide phosphodiesterase, Gene 234 (1999) 109–117.
[12] H. Wang, Y. Liu, J. Hou, M. Zheng, H. Robinson, H. Ke, Structural insight into substrate specificity of phosphodiesterase 10, Proc. Natl. Acad. Sci. U. S. A. 104 (2007) 5782–5787.
[13] N. Handa, E. Mizohata, S. Kishishita, M. Toyama, S. Morita, T. Uchikubo-Kamo, et al., Crystal structure of the GAF-B domain from human phosphodiesterase 10A complexed with its ligand, cAMP, J. Biol. Chem. 283 (2008) 19657–19664.
[14] A. Chino, N. Masuda, Y. Amano, K. Honbou, T. Mihara, M. Yamazaki, et al., Novel benzimidazole derivatives as phosphodiesterase 10A (PDE10A) inhibitors with improved metabolic stability, Bioorg. Med. Chem. 22 (2014) 3515–3526.
[15] E. Hu, R.K. Kunz, N. Chen, S. Rumfelt, A. Siegmund, K. Andrews, et al., Design, optimization, and biological evaluation of novel keto-benzimidazoles as potent and selective inhibitors of phosphodiesterase 10A (PDE10A), J. Med. Chem. 56 (2013) 8781–8792.
[16] E. Hu, R.K. Kunz, S. Rumfelt, N. Chen, R. Burli, C. Li, et al., Discovery of potent, selective, and metabolically stable 4-(pyridin-3-yl) cinnolines as novel phosphodiesterase 10A (PDE10A) inhibitors, Bioorg. Med. Chem. Lett. 22 (2012) 2262–2265.
[17] J. Kehler, A. Ritzen, M. Langgard, S.L. Petersen, M.M. Farah, C. Bundgaard, et al., Triazoloquinazolines as a novel class of phosphodiesterase 10A (PDE10A) inhibitors, Bioorg. Med. Chem. Lett. 21 (2011) 3738–3742.
[18] M.I. Recht, V. Sridhar, J. Badger, P.Y. Bounaud, C. Logan, B. Chie-Leon, et al., Identification and optimization of PDE10A inhibitors using fragment-based screening by nanocalorimetry and X-ray crystallography, J. Biomol. Screen. 19 (2014) 497–507.
[19] S.W. Yang, J. Smotryski, W.T. McElroy, Z. Tan, G. Ho, D. Tulshian, et al., Discovery of orally active pyrazoloquinolines as potent PDE10 inhibitors for

the management of schizophrenia, Bioorg. Med. Chem. Lett. 22 (2012) 235–239.
[20] M.S. Malamas, Y. Ni, J. Erdei, H. Stange, R. Schindler, H.J. Lankau, et al., Highly potent, selective, and orally active phosphodiesterase 10A inhibitors, J. Med. Chem. 54 (2011) 7621–7638.
[21] E. Hu, N. Chen, M.P. Bourbeau, P.E. Harrington, K. Biswas, R.K. Kunz, et al., Discovery of clinical candidate 1-(4-(3-(4-(1H-benzo[d]imidazole-2-carbonyl) phenoxy) pyrazin-2-yl) piperidin-1-yl) e thanone (AMG 579), a potent, selective, and efficacious inhibitor of phosphodiesterase 10A (PDE10A), J. Med. Chem. 57 (2014) 6632–6641.
[22] J. Kehler, J.P. Kilburn, Patented PDE10A inhibitors: novel compounds since 2007, Expert Opin. Ther. Pat. 19 (2009) 1715–1725.
[23] J. Kehler, A. Ritzén, D.R. Greve, The potential therapeutic use of phosphodiesterase 10 inhibitors, Expert Opin. Ther. Pat. 17 (2007) 147–158.
[24] J. Aqvist, V.B. Luzhkov, B.O. Brandsdal, Ligand binding affinities from MD simulations, Acc. Chem. Res. 35 (2002) 358–365.
[25] J. Aqvist, C. Medina, J. Samuelsson, A new method for predicting binding affinity in computer-aided drug design, Protein Eng. 7 (1994) 385–391.
[26] S. Liu, L.H. Zhou, H.Q. Wang, Z.B. Yao, Superimposing the 27 crystal protein/inhibitor complexes of beta-secretase to calculate the binding affinities by the linear interaction energy method, Bioorg. Med. Chem. Lett. 20 (2010) 6533–6537.
[27] A. de Ruiter, C. Oostenbrink, Free energy calculations of protein-ligand interactions, Curr. Opin. Chem. Biol. 15 (2011) 547–552.
[28] M.K. Gilson, H.X. Zhou, Calculation of protein-ligand binding affinities, Ann. Rev. Biophys. Biomol. Struct. 36 (2007) 21–42.
[29] M.R. Reddy, C.R. Reddy, R.S. Rathore, M.D. Erion, P. Aparoy, R.N. Reddy, et al., Free energy calculations to estimate ligand-binding affinities in structure-based drug design, Curr. Pharm. Des. 20 (2014) 3323–3337.
[30] B.O. Brandsdal, F. Osterberg, M. Almlof, I. Feierberg, V.B. Luzhkov, J. Aqvist, Free energy calculations and ligand binding, Adv. Protein Chem. 66 (2003) 123–158.
[31] E. Stjernschantz, J. Marelius, C. Medina, M. Jacobsson, N.P. Vermeulen, C. Oostenbrink, Are automated molecular dynamics simulations and binding free energy calculations realistic tools in lead optimization? An evaluation of the linear interaction energy (LIE) method, J. Chem. Inf. Model. 46 (2006) 1972–1983.
[32] E. Stjernschantz, C. Oostenbrink, Improved ligand–protein binding affinity predictions using multiple binding modes, Biophys. J. 98 (2010) 2682–2691.
[33] R. Zhou, R.A. Friesner, A. Ghosh, R.C. Rizzo, W.L. Jorgensen, R.M. Levy, New linear interaction method for binding affinity calculations using a continuum solvent model, J. Phys. Chem. B 105 (2001) 10388–10397.
[34] P. Kolb, D. Huang, F. Dey, A. Caflisch, Discovery of kinase inhibitors by high-throughput docking and scoring based on a transferable linear interaction energy model, J. Med. Chem. 51 (2008) 1179–1188.
[35] R.C. Rizzo, M. Udier-Blagovic, D.P. Wang, E.K. Watkins, M.B. Kroeger Smith, R.H. Smith Jr, et al., Prediction of activity for nonnucleoside inhibitors with HIV-1 reverse transcriptase based on Monte Carlo simulations, J. Med. Chem. 45 (2002) 2970–2987.
[36] Liaison. Schrödinger LLC., Portland, US. http://www.schrodinger.com
[37] Maestro (version 9.6), Schrödinger LLC., Portland, USA. http://www.schrodinger.com, 2013.
[38] A. Bortolato, S. Moro, In silico binding free energy predictability by using the linear interaction energy (LIE) method: bromobenzimidazole CK2 inhibitors as a case study, J. Chem. Inf. Model. 47 (2007) 572–582.
[39] Impact (version 6.2), Schrödinger, LLC, New York, NY, 2014. 2013.
[40] S.S. Kulkarni, M.R. Patel, T.T. Talele, CoMFA and HQSAR studies on 6,7-dimethoxy-4-pyrrolidylquinazoline derivatives as phosphodiesterase10A inhibitors, Bioorg. Med. Chem. 16 (2008) 3675–3686.
[41] LigPrep (version 10.3), Schrödinger LLC., Portland, USA. http://www.schrodinger.com, 2013.
[42] J.R. Greenwood, D. Calkins, A.P. Sullivan, J.C. Shelley, Towards the comprehensive, rapid, and accurate prediction of the favorable tautomeric states of drug-like molecules in aqueous solution, J. Comput. Aided Mol. Des. 24 (2010) 591–604.
[43] G.M. Sastry, M. Adzhigirey, T. Day, R. Annabhimoju, W. Sherman, Protein and ligand preparation: parameters, protocols, and influence on virtual screening enrichments, J. Comput. Aided Mol. Des. 27 (2013) 221–234.
[44] H. Li, A.D. Robertson, J.H. Jensen, Very fast empirical prediction and rationalization of protein pKa values, Proteins 61 (2005) 704–721.
[45] R.A. Friesner, J.L. Banks, R.B. Murphy, T.A. Halgren, J.J. Klicic, D.T. Mainz, et al., Glide: a new approach for rapid, accurate docking and scoring. 1. Method and assessment of docking accuracy, J. Med. Chem. 47 (2004) 1739–1749.
[46] W. Sippl, 3D-QSAR–Applications, Recent Advances, and Limitations, in: P. Tomasz, L. Jerzy, C.T. Mark (Eds.), In Recent Advances in New York, Springer QSAR Studies: Methods and Applications, 8th ed., Springer, New York, 2010.
[47] A. Tropsha, P. Gramatica, V.K. Gombar, The importance of being earnest: validation is the absolute essential for successful application and interpretation of QSPR models, QSAR Comb. Sci. 22 (2003) 69–77.
[48] A.P. Bento, A. Gaulton, A. Hersey, L.J. Bellis, J. Chambers, M. Davies, et al., The ChEMBL bioactivity database: an update, Nucleic Acids Res. 42 (2014) D1083–D1090.
[49] T.A. Chappie, C.J. Helal, X. Hou, Current landscape of phosphodiesterase 10A (PDE10A) inhibition, J. Med. Chem. 55 (2012) 7299–7331.
[50] G.D. Ho, W. Michael Seganish, A. Bercovici, D. Tulshian, W.J. Greenlee, R. Van Rijn, et al., The SAR development of dihydroimidazoisoquinoline derivatives as phosphodiesterase 10A inhibitors for the treatment of schizophrenia, Bioorg. Med. Chem. Lett. 22 (2012) 2585–2589.
[51] G.D. Ho, S.W. Yang, J. Smotryski, A. Bercovici, T. Nechuta, E.M. Smith, et al., The discovery of potent, selective, and orally active pyrazoloquinolines as PDE10A inhibitors for the treatment of Schizophrenia, Bioorg. Med. Chem. Lett. 22 (2012) 1019–1022.
[52] W.T. McElroy, Z. Tan, K. Basu, S.W. Yang, J. Smotryski, G.D. Ho, et al., Pyrazoloquinolines as PDE10A inhibitors: discovery of a tool compound, Bioorg. Med. Chem. Lett. 22 (2012) 1335–1339.
[53] I.T. Raheem, M.J. Breslin, C. Fandozzi, J. Fuerst, N. Hill, S. Huszar, et al., Discovery of tetrahydropyridopyrimidine phosphodiesterase 10A inhibitors for the treatment of schizophrenia, Bioorg. Med. Chem. Lett. 22 (2012) 5903–5908.
[54] J.J. Irwin, T. Sterling, M.M. Mysinger, E.S. Bolstad, R.G. Coleman, Zinc a free tool to discover chemistry for biology, J. Chem. Inf. Model. 52 (2012) 1757–1768.
[55] J.A. Grant, M.A. Gallardo, B.T. Pickup, A fast method of molecular shape comparison: a simple application of a Gaussian description of molecular shape, J. Comput. Chem. 17 (1996) 1653–1666.
[56] vROC. OEChem, version 1.7.2, OpenEye Scientific Software, Inc., Santa Fe, NM, USA, http://www.eyesopen.com, 2013.
[57] Canvas. Schrödinger, LLC, New York, USA, 2013.